Electronic Supplementary Information for *New Journal of Chemistry*

Design of $Cu/ZnO/Al_2O_3$ catalysts with rich Cu-ZnO interface for enhanced CO_2 hydrogenation to methanol using zinc-malachite as precursor

Haotian Zhang [a], Caiyun Han [a], Congming Li [c], Peng Wang [a, b *], Hao Huang [d], Shuang Wang [a, b, *], Jinping Li [b]

[a] College of Environmental Science and Engineering, Taiyuan University of Technology, Jinzhong 030600, Shanxi, P.R. China.

[b] Shanxi Key Laboratory of Gas Energy Efficient and Clean Utilization, Taiyuan University of Technology, Taiyuan 030024, Shanxi, P.R. China.

[c] State Key Laboratory of Clean and Efficient Coal Utilization, Taiyuan University of Technology, Taiyuan 030024, Shanxi, China.

[d] Department of Microsystems, University of South-Eastern Norway, Borre 3184, Norway.

E-mails: wangshuang@tyut.edu.cn, wangpeng01@tyut.edu.cn

Contents

Section S1 Materials characterization

Powder X-ray Diffraction (XRD): XRD patterns were analyzed on a Bruker D8 Advance X-ray diffractometer using Cu Kα radiation (40 kV, 40 mA, λ = 0.15418 nm) with a scan rate of $8°\cdot min^{-1}$ and a 2θ range of 10-50° for precursors and 10-80° for catalysts.

Inductively Coupled Plasma Optical Emission Spectrometer (ICP-OES): Elemental content data for Cu, Zn, and Al were obtained by a PerkinElmer Avio 200 ICP-OES instrument. Samples were digested as described below. A 10 mg sample was dispersed in 10 mL of phosphoric acid and then diluted to 100 mL with deionized water prior to measurement.

Nitrogen adsorption and desorption isotherms: N_2 adsorption-desorption measurements were performed by nitrogen adsorption (-77 k) on a Micromeritics TriStar II 3020 instrument. Prior to testing, samples were vacuum dried at 200°C for 10 h. Surface areas were calculated using the Brunauer-Emmett-Teller (BET) method.

Transmission electron microscopy (TEM): TEM samples were prepared by dispersing the samples in ethanol using a sonic bath followed by drop casting onto copper grid. The TEM images and EDS mapping were performed using JEM-2100F with an accelerating voltage of 200 kV.

X-ray photoelectron spectroscopy (XPS): XPS measurements were performed on a Thermo Fisher Scientific K-Alpha spectrometer with Al Ka (1486.8 eV) as the X-ray source. The samples used for testing were CZA-1-R, CZA-2-R and CZA-3-R.

Temperature-programmed H_2 reduction (H_2-TPR): H_2-temperature programmed reduction (H_2-TPR) was carried out using Micromeritics AutoChem II 2920 chemisorption analyzer. Before the H_2-TPR test, the calcined sample of 50 mg was

heated to 150°C under Ar atmosphere (30 mL·min^{-1}) and purged for 1 h, and then cooled to 50°C. The reduction process was performed in the range of 50-400°C under 10% H_2/Ar (30 mL·min^{-1}) atmosphere.

Temperature-programmed CO_2 desorption (CO_2-TPD): CO_2-TPD were carried out using a Micromeritics AutoChem II 2920 chemisorption instrument. Before the CO_2-TPD test, the reduced sample of 50 mg was heated to 150°C under He atmosphere (30 mL·min^{-1}) and purged for 1 h. After being cooled to 50°C in a He atmosphere, the sample was purged with 10% CO_2/He mixture (30 mL·min^{-1}) for 1.5 h at 50°C to saturate the surface, then purged in flowing He (30 mL·min^{-1}) for 1.5 h to remove physically adsorbed CO_2. Subsequently, the temperature was elevated in flowing He (30 mL·min^{-1}) until up to 800°C at a ramp rate of 10°C·min^{-1}. CO_2 desorption amount was quantitatively measured based on CO_2 single-pulse experiment.

Temperature-programmed H_2 desorption (H_2-TPD): H_2-TPD were carried out using a Micromeritics AutoChem II 2920 chemisorption instrument. H_2-TPD experiment was carried out with the similar method as that employed in CO_2-TPD. Before the H_2-TPD test, the reduced sample of 50 mg was heated to 150°C under Ar atmosphere (30 mL·min^{-1}) and purged for 1 h. After being cooled to 50°C in an Ar atmosphere, the sample was purged with 10% H_2/Ar mixture (30 mL·min^{-1}) for 1.5 h at 50°C to saturate the surface, then purged in flowing Ar (30 mL·min^{-1}) for 1.5 h to remove physically adsorbed H_2. Subsequently, the temperature was elevated in flowing Ar (30 mL·min^{-1}) until up to 800°C at a ramp rate of 10°C·min^{-1}. The desorbed H_2 signal was monitored by a TCD detector, and H_2 desorption amount was quantitatively calculated by H_2 single-pulse experiment.

Cu dispersion (D_{Cu}) and metallic Cu special surface area (S_{Cu}): Assuming that the

chemisorption of H on copper atoms proceeds according to Cu:H = 2:1, the specific surface area (S_{Cu}) and dispersion D_{Cu}) of copper are calculated as follows:

$$S_{Cu} = 4 \times H_2\text{uptake} \times N_{av}/(1.47 \times 10^{19})(m^2/g)$$

In this equation, N av is Avogadro's constant and 1.47×10^{19} is the value of Cu atoms per square meter [1].

$$D_{Cu} = \frac{\text{amount of Cu atoms on surface (moles)}}{\text{total amount of Cu atoms on sample (moles)}} \times 100\%$$

$$= \frac{H_2\text{uptake} \times 4(\text{moles})}{\text{total amount of Cu atoms on sample (moles)}} \times 100\%$$

Section S2 Catalytic performance measurement

Activity measurements in the hydrogenation of CO_2 were carried out in a fixed-bed reactor. Calcined sample (CZA-C, 0.4 g, 40 - 60 mesh) diluted with 1.1 g quartz sand (40 - 60 mesh) was placed in a stainless steel tube reactor. Prior to reaction, the sample was reduced in H_2/N_2 (10/90, v/v) mixture gas at a flow-rate of 60 mL min^{-1} under atmospheric pressure. The reduction temperature was programmed to increase from room temperature to 290°C and maintained at 290°C for 4 h. The reactor was then cooled to room temperature. After reduction, the activities of the catalyst samples in CO_2 hydrogenation process were determined under specific reaction conditions.

The exit gas from the reactor was maintained at 150°C and immediately transported to the sample valve of the GC (Agilent 8860), which was equipped with thermal conductivity (TCD) and flame ionization detectors (FIDs). TDX-01 C molecular sieve packed columns (1 m × 3 mm; Agilent) were connected to TCD, whereas HP-PLOT/Q capillary columns were connected to FID. The packed column was used for the analysis of CO_2 and CO, and the capillary column (30 m × 0.32 mm × 20 μm; Agilent Technologies, Inc) was used for methanol (CH_3OH), methoxymethane (CH_3OCH_3), methane (CH_4) and other C-containing products. CO_2 conversion (denoted as X_{CO_2}), the CH_3OH selectivity (denoted as S_{CH_3OH}) and the yield of CH_3OH were calculated using an external normalization method, which were defined as the following Eq. 1, Eq. 2, and Eq. 3.

$$X_{CO_2}(\%) = \frac{n(CO) + n(CH_4) + n(CH_3OH)}{n(CO) + n(CH_4) + n(CH_3OH) + n(CO_2)} \times 100 \quad \text{Eq. 1}$$

$$S_{CH_3OH}(\%) = \frac{n(CH_3OH)}{n(CH_3OH) + n(CO) + n(CH_4)} \times 100 \quad \text{Eq. 2}$$

$$Yield_{CH_3OH}(\%) = X_{CO_2} \times S_{CH_3OH} \times 100 \quad \text{Eq. 3}$$

Section S3 Attached drawings and schedules

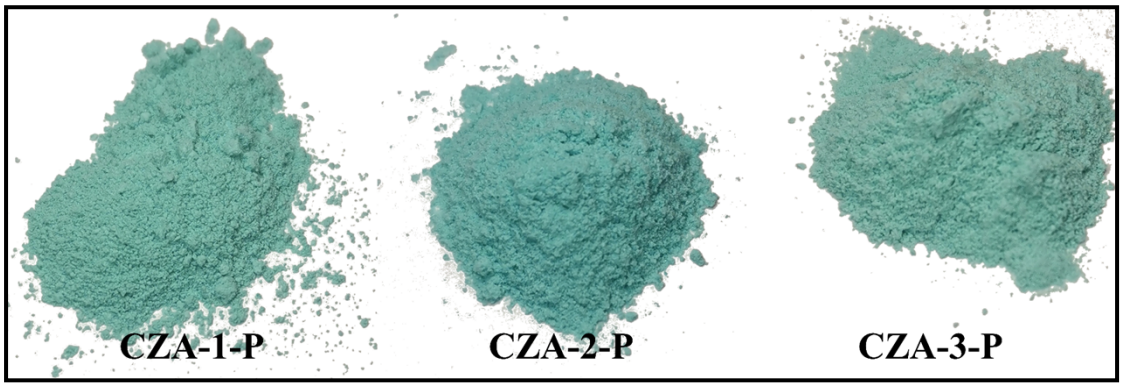

Photo S1. Photos of precursors and calcined samples.

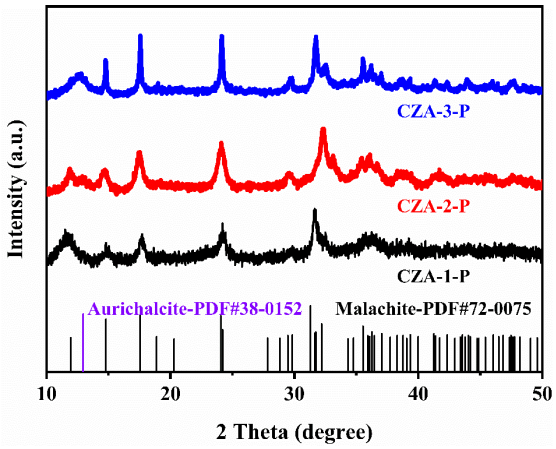

Fig. S1. XRD patterns of CZA-1-P, CZA-2-P and CZA-3-P.

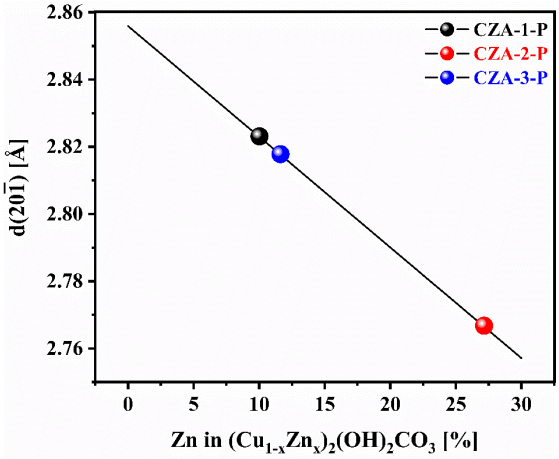

Fig. S2. The lattice plane reflection characteristics and zinc substitutions amount of CZA-1-P, CZA-2-P and CZA-3-P.

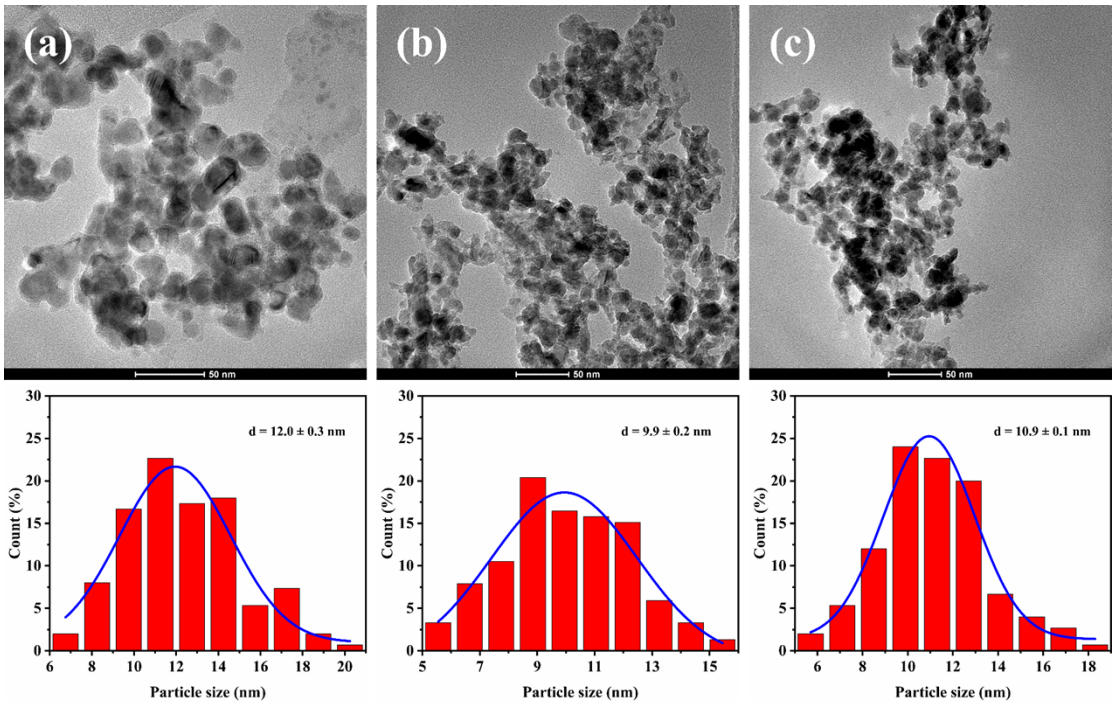

Fig. S3. TEM images and histograms of particle size statistical distribution of various catalysts: (a) CZA-1-R; (b) CZA-2-R; (c) CZA-3-R. (The particle size count is 150 for each image).

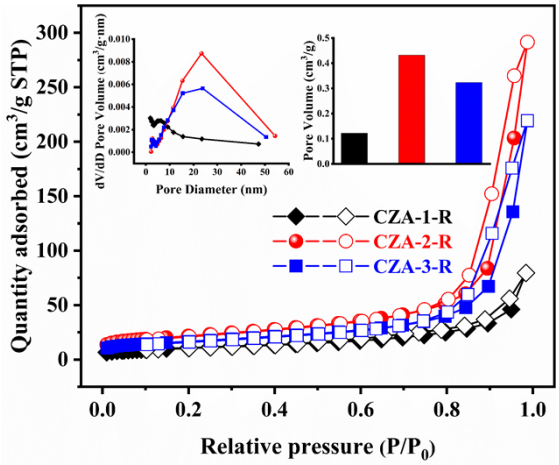

Fig. S4. N_2 adsorption-desorption isotherms of the CZA-1-R, CZA-2-R and CZA-3-R.

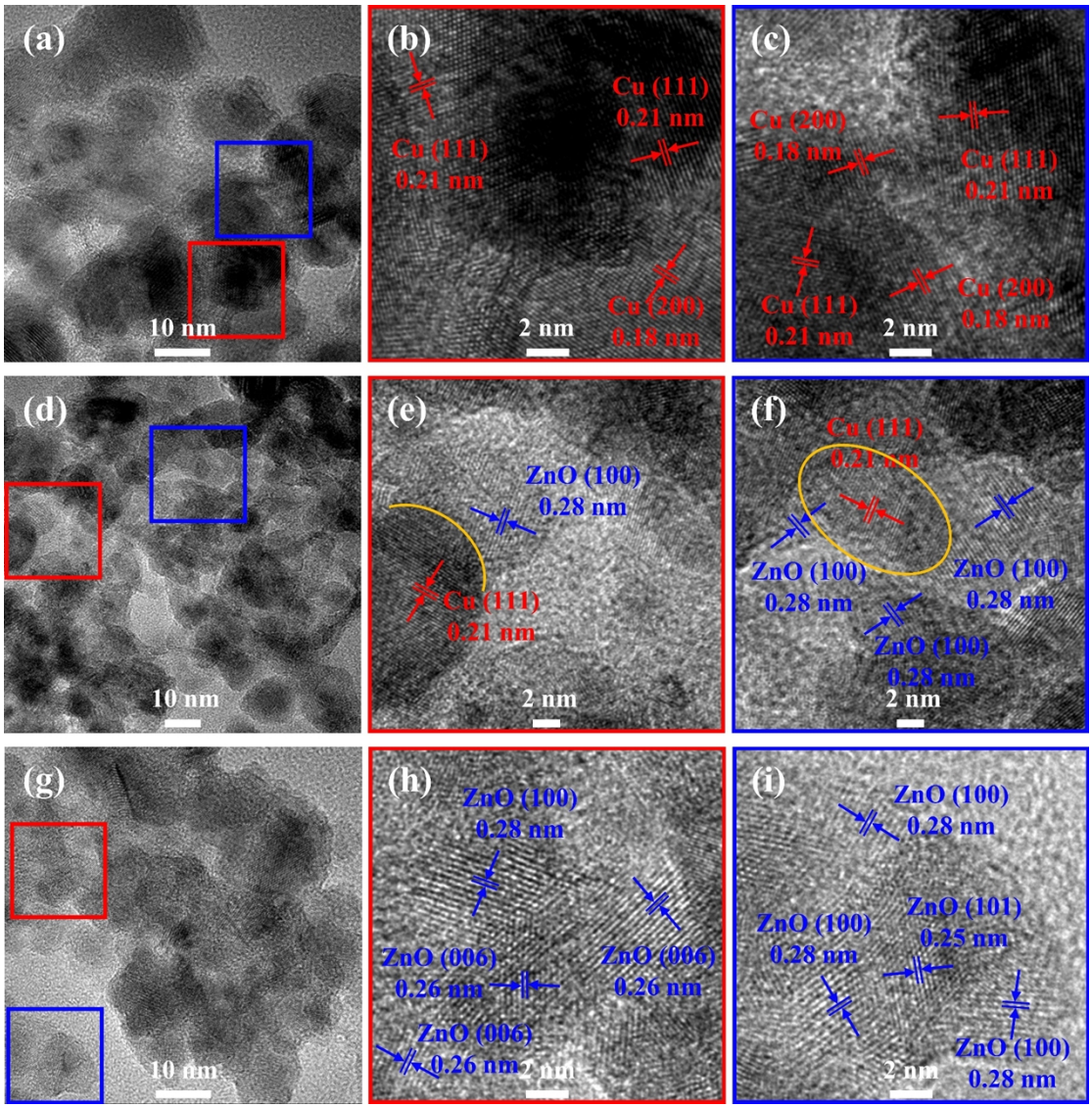

Fig. S5. HRTEM images of CZA-1-R (a-c), CZA-2-R (d-f), CZA-3-R (g-i). (Yellow lines represent Cu-ZnO interface)

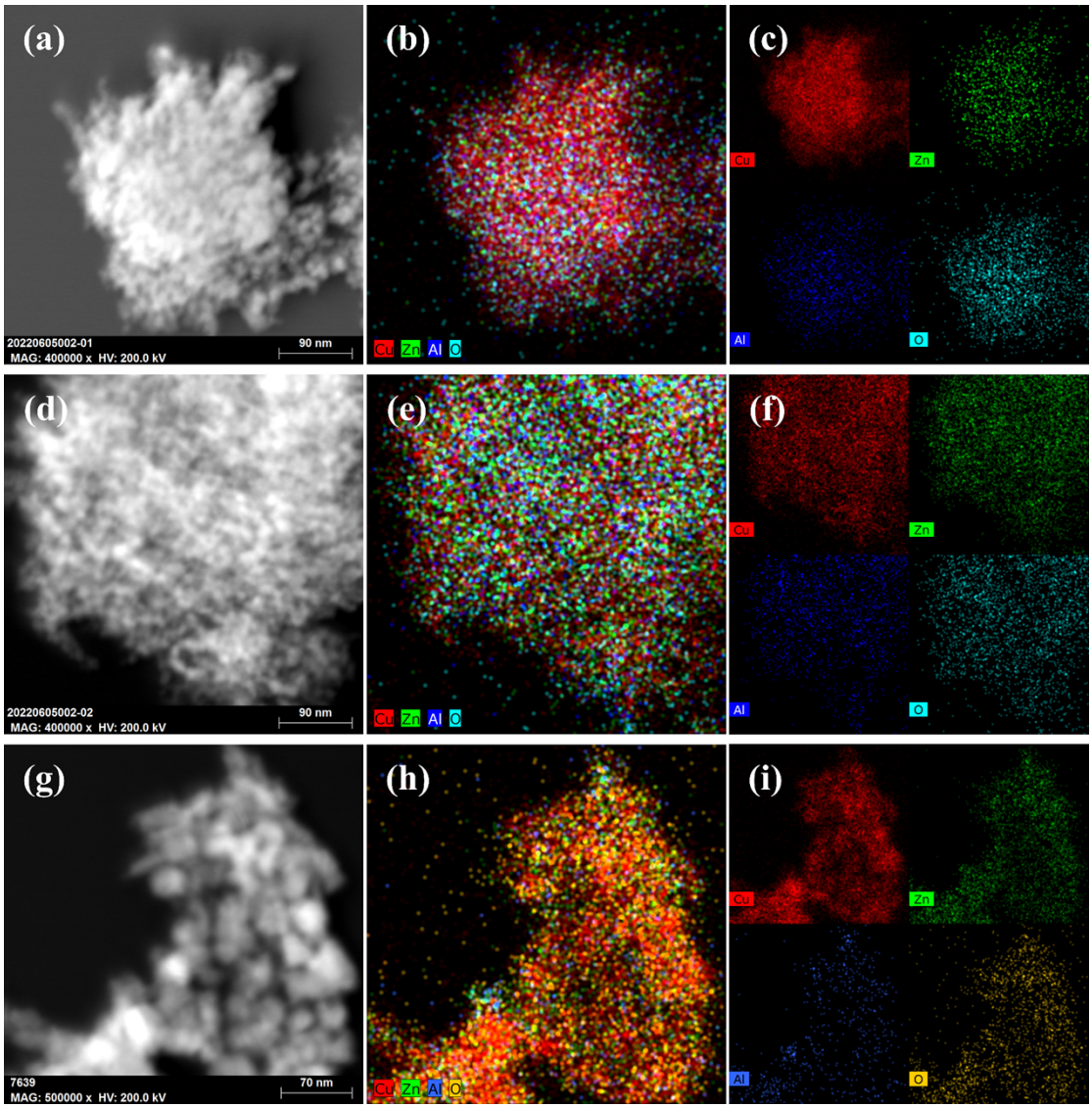

Fig. S6. HAADF-STEM images and EDS elemental mappings of Cu, Zn, Al and O for CZA-1-R (a-c), CZA-2-R (d-f) and CZA-3-R (g-i).

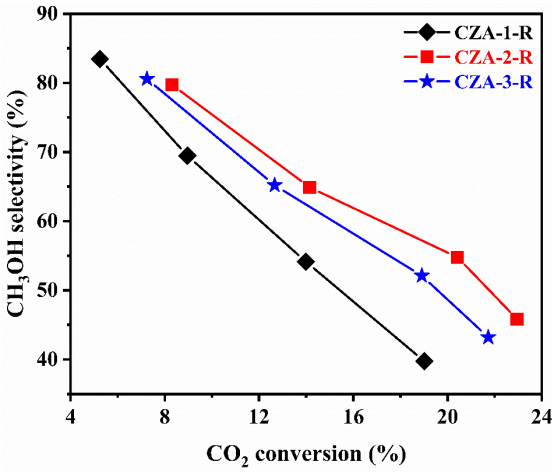

Fig. S7 Relationship between CO_2 conversion and methanol selectivity in CZA-1-R, CZA-2-R and CZA-3-R.

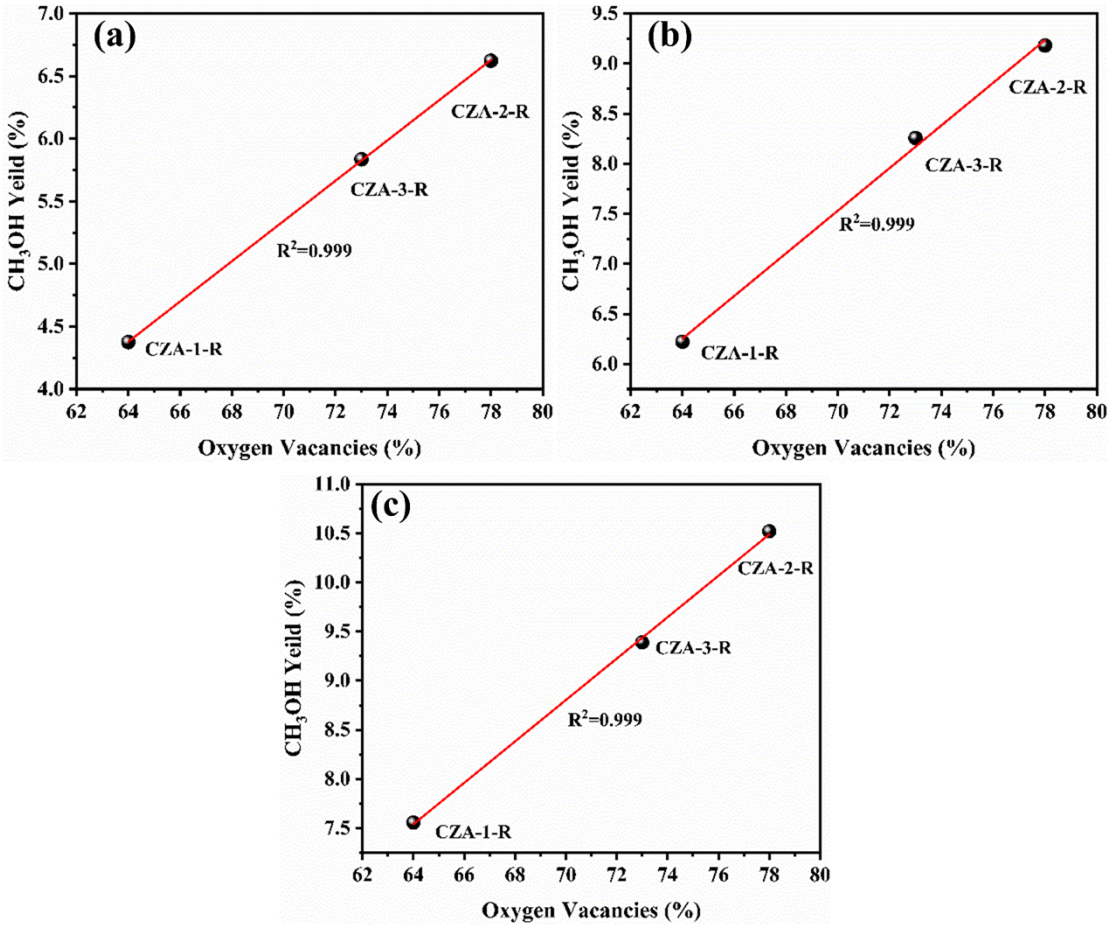

Fig. S8. The relationship between the concentration of oxygen vacancies relative to the methanol yield at (a) 190°C, (b) 210°C, (c) 250°C over different catalysts. Reaction conditions: 3 MPa, $V_{H2/CO2}$ = 3 and WHSV = 10000 $mL \cdot g_{cat}^{-1} \cdot h^{-1}$.

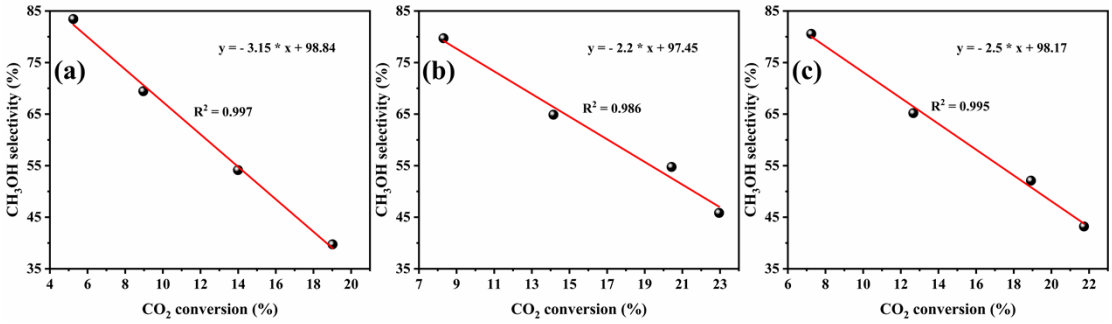

Fig. S9. The relationship between CO_2 conversion and methanol selectivity in (a) CZA-1-R, (b) CZA-2-R and (c) CZA-3-R. Reaction conditions: 3 MPa, $V_{H2/CO2}$ = 3 and WHSV = 10000 mL·g_{cat}^{-1}·h^{-1}.

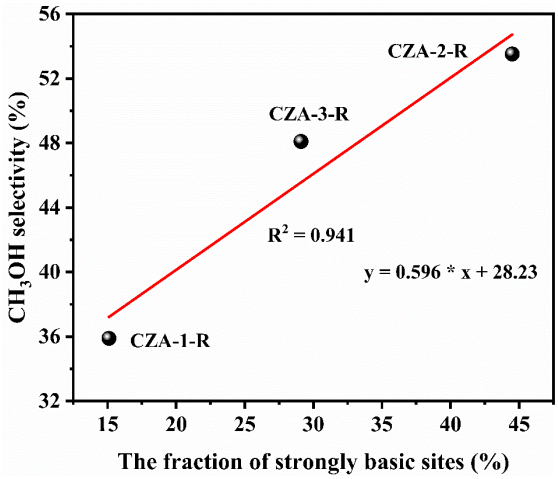

Fig. S10. The relationship between the fraction of strongly basic sites relative to all the basic sites and methanol selectivity over the different catalysts at the 20% CO_2 conversion. Reaction conditions: 3 MPa, $V_{H2/CO2}$ = 3 and WHSV = 10000 mL·g_{cat}^{-1}·h^{-1}.

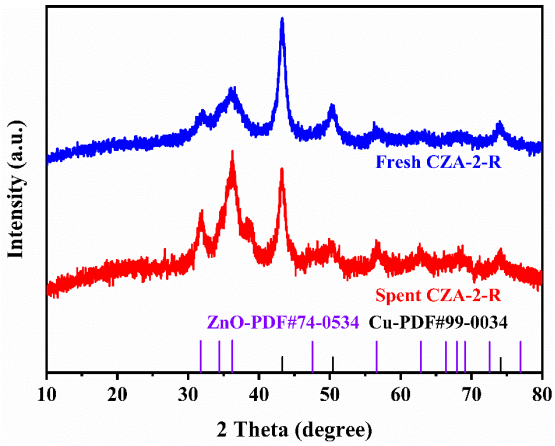

Fig. S11. XRD patterns of fresh CZA-2-R and CZA-2-R after 120 h stability test.

Table S1

Catalytic performance of $Cu/ZnO/Al_2O_3$ catalysts in CO_2 hydrogenation to CH_3OH.

Catalyst	Preparation method	H_2/CO_2	P (MPa)	T (°C)	SV	X_{CO_2} (%)	S_{CH_3OH} (%)	Yield (%)	Ref
$Cu/ZnO/Al_2O_3$	Co-precipitation	3	3	190	10000 $mL \cdot g_{cat}^{-1} \cdot h^{-1}$	8.31	79.7	6.6	This work
				210		14.15	64.9	9.2	
				230		20.4	54.8	11.2	
				250		23.0	45.8	10.5	
Cu/Zn/Al-HT	-	3	3	250	2600 $mL \cdot g_{cat}^{-1} \cdot h^{-1}$	6	73.4	4.4	2
Cu/Zn/Al/Zr	Co-precipitation	3	4	240	9742 h^{-1}	18.7	47.2	8.8	3
Cu/Zn/Zr	Co-precipitation	3	3	200	8800 h^{-1}	5.8	55.2	3.2	4
Cu/Zn/Al	Co-precipitation	3	3	230	-	18.7	43	8.0	5
Cu/Zn/Al- commercial catalyst	-	3	4	250	18000 h^{-1}	11.1	54.8	6.1	6
Cu/Zn/Al-LDO	Hydrothermal	3	3	250	-	7	50	3.5	7
$Cu\text{-}ZnO^{MOF} \subset Al_2O_3$	Solvothermal	3	3	240	14400 h^{-1}	9.1	86.9	7.9	8
$Cu\text{-}ZnO/Al_2O_3$	Co-precipitation	3	3	240	14400 h^{-1}	5.1	79.6	4.1	8
$Cu\text{-}ZnO@Al_2O_3$	Co-precipitation	3	3	250	1500 $mL \cdot g_{cat}^{-1} \cdot h^{-1}$	19.8	48	9.5	9
10NG-Cu/Zn/Al	Co-precipitation	3	3	200	-	8.2	84	6.8	10
Cu/Zn/Al	Ultrasonic co-precipitation	3	2	200	2000 h^{-1}	5	66	3.3	11
$Cu/Zn/\gamma\text{-}Al_2O_3$	Ammonia deposition-precipitation	3	4	220	1500 $mL \cdot g_{cat}^{-1} \cdot h^{-1}$	15	58.9	8.8	12
$Cu/ZnO/Al_2O_3$	Co-precipitation	3	5	230	2500 $mL \cdot g_{cat}^{-1} \cdot h^{-1}$	27.5	75	20.66	This work
Cu/Zn/Al	Co-precipitation	2.8	5	170	400 $mL \cdot g_{cat}^{-1} \cdot h^{-1}$	14.3	54.8	7.8	13
$Cu/ZnO/Al_2O_3$	Precipitation	2.2	4.5	280	8000 $mL \cdot g_{cat}^{-1} \cdot h^{-1}$	12	71.6	8.6	14
Cu/Zn/Zr	Co-precipitation	3.89	5	280	10000 h^{-1}	21	34	7.1	15
Cu/Zn/Al/Zr	Co-precipitation	3	5	190	4000 h^{-1}	18.9	81.1	15.3	16
Cu/Zn/Al/Zr	Co-precipitation	3	5	250	4000 h^{-1}	25.6	61.3	15.7	17

Table S2

The stability of over the reported catalysts for CO_2 hydrogenation to methanol.

Catalysts	Before stability test		After stability test		Time on stream	Ref.
	CO_2 Conv. (%)	CH_3OH Sel. (%)	CO_2 Conv. (%)	CH_3OH Sel. (%)		
CZA-2-R	20	54.5	20	54.3	120	This work
CZZ	~17.0	~45.5	~15	~45.5	100	18
CZ/Z	15.8	40.4	-	-	100	19
Cu/SiO_2	20	23	-	-	45	20
CZS-0	14	30	11.7	30.2	41.6	21
CZZ-400	16.8	41	16.1	42	130	22
$C_5Z_2Z_{2.8}W_{0.2}$	19.7	49.3	~19.3	~48	100	23
CZZ-120	~18.4	~37.5	~17.3	~36	100	24
CZZ-flower	~19	~57	~18	~59	100	25

Reference

1. G. Wang, F. Luo, L. Lin and F. Zhao, *React. Kinet., Mech. Catal.*, 2021, **132**, 155-170.
2. X. Fang, Y. Men, F. Wu, Q. Zhao, R. Singh, P. Xiao, T. Du and P. A. Webley, *Chem. Eng. J.*, 2019, **378**, 122052.
3. X. An, J. Li, Y. Zuo, Q. Zhang, D. Wang and J. Wang, *Catal. Lett.*, 2007, **118**, 264-269.
4. F. Arena, K. Barbera, G. Italiano, G. Bonura, L. Spadaro and F. Frusteri, *J. Catal.*, 2007, **249**, 185-194.
5. C. Li, X. Yuan and K. Fujimoto, *Appl. Catal. A Gen.*, 2014, **469**, 306-311.
6. B. An, J. Zhang, K. Cheng, P. Ji, C. Wang and W. Lin, *J. Am. Chem. Soc.*, 2017, **139**, 3834-3840.
7. F. Zhao, L. Fan, K. Xu, D. Hua, G. Zhan and S. Zhou, *J. CO_2 Util.*, 2019, **33**, 222-232.
8. T. Qi, Y. Zhao, S. Chen, W. Li, X. Guo, Y. Zhang and C. Song, *Mol. Catal.*, 2021, **514**.
9. T. T. N. Hoang, Y.-S. Lin, T. N. H. Le, T. K. Le, T. K. X. Huynh and D. Tsai, *Adv. Powder Technol.*, 2021, **32**, 1785-1792.
10. Q. Ma, M. Geng, J. Zhang, X. Zhang and T. Zhao, *ChemistrySelect*, 2019, **4**, 78-83.
11. V. D. B. C. Dasireddy and B. Likozar, *Renew. Energy*, 2019, **140**, 452-460.
12. C. Zhang, H. Yang, P. Gao, H. Zhu, L. Zhong, H. Wang, W. Wei and Y. Sun, *J. CO_2 Util.*, 2017, **17**, 263-272.
13. Y. Liu, Y. Zhang, T. Wang and N. Tsubaki, *Chem. Lett.*, 2007, **36**, 1182-1183.
14. F. Liao, Y. Huang, J. Ge, W. Zheng, K. Tedsree, P. Collier, X. Hong and S. C. Tsang, *Angew Chem Int Ed Engl*, 2011, **50**, 2162-2165.
15. L. Angelo, M. Girleanu, O. Ersen, C. Serra, K. Parkhomenko and A.-C. Roger, *Catal. Today*, 2016, **270**, 59-67.
16. S. Xiao, Y. Zhang, P. Gao, L. Zhong, X. Li, Z. Zhang, H. Wang, W. Wei and Y. Sun, *Catal. Today*, 2017, **281**, 327-336.
17. P. Gao, R. Xie, H. Wang, L. Zhong, L. Xia, Z. Zhang, W. Wei and Y. Sun, *J. CO_2 Util.*, 2015, **11**, 41-48.
18. Y. Liang, D. Mao, X. Guo, J. Yu, G. Wu and Z. Ma, *J. Taiwan Inst. Chem. Eng.*, 2021, **121**, 81-91.
19. J. Yu, G. Chen, Q. Guo, X. Guo, P. Da Costa and D. Mao, *Fuel*, 2022, **324**.
20. Z. Yan, Y. Wang, X. Wang, C. Xu, W. Zhang, H. Ban and C. Li, *Catal. Lett.*, 2022, DOI: 10.1007/s10562-022-04047-7.
21. Y. Wang, X. Wang, Z. Yan, C. Xu, W. Zhang, H. Ban and C. Li, *J. Catal.*, 2022, **412**, 10-20.
22. D. Chen, D. Mao, G. Wang, X. Guo and J. Yu, *J. Sol-Gel Sci. Technol.*, 2019, **89**, 686-699.
23. G. Wang, D. Mao, X. Guo and J. Yu, *Appl. Surf. Sci.*, 2018, **456**, 403-409.
24. C. Huang, D. Mao, X. Guo and J. Yu, *Energy Technol.*, 2017, **5**, 2100-2107.
25. H. Chen, H. Cui, Y. Lv, P. Liu, F. Hao, W. Xiong and H. a. Luo, *Fuel*, 2022, **314**, 123035.